On the interstitial induced lattice inhomogeneities in nitrogen-expanded austenite

Tao, Xiao; Qi, Jiahui; Rainforth, Mark; Matthews, Allan; Leyland, Adrian

DOI:
10.1016/j.scriptamat.2020.04.045

Document Version
Peer reviewed version

Citation for published version (Harvard):
Tao, X, Qi, J, Rainforth, M, Matthews, A & Leyland, A 2020, 'On the interstitial induced lattice inhomogeneities in nitrogen-expanded austenite', *Scripta Materialia*, vol. 185, pp. 146-151.
https://doi.org/10.1016/j.scriptamat.2020.04.045

*Graphical Abstract

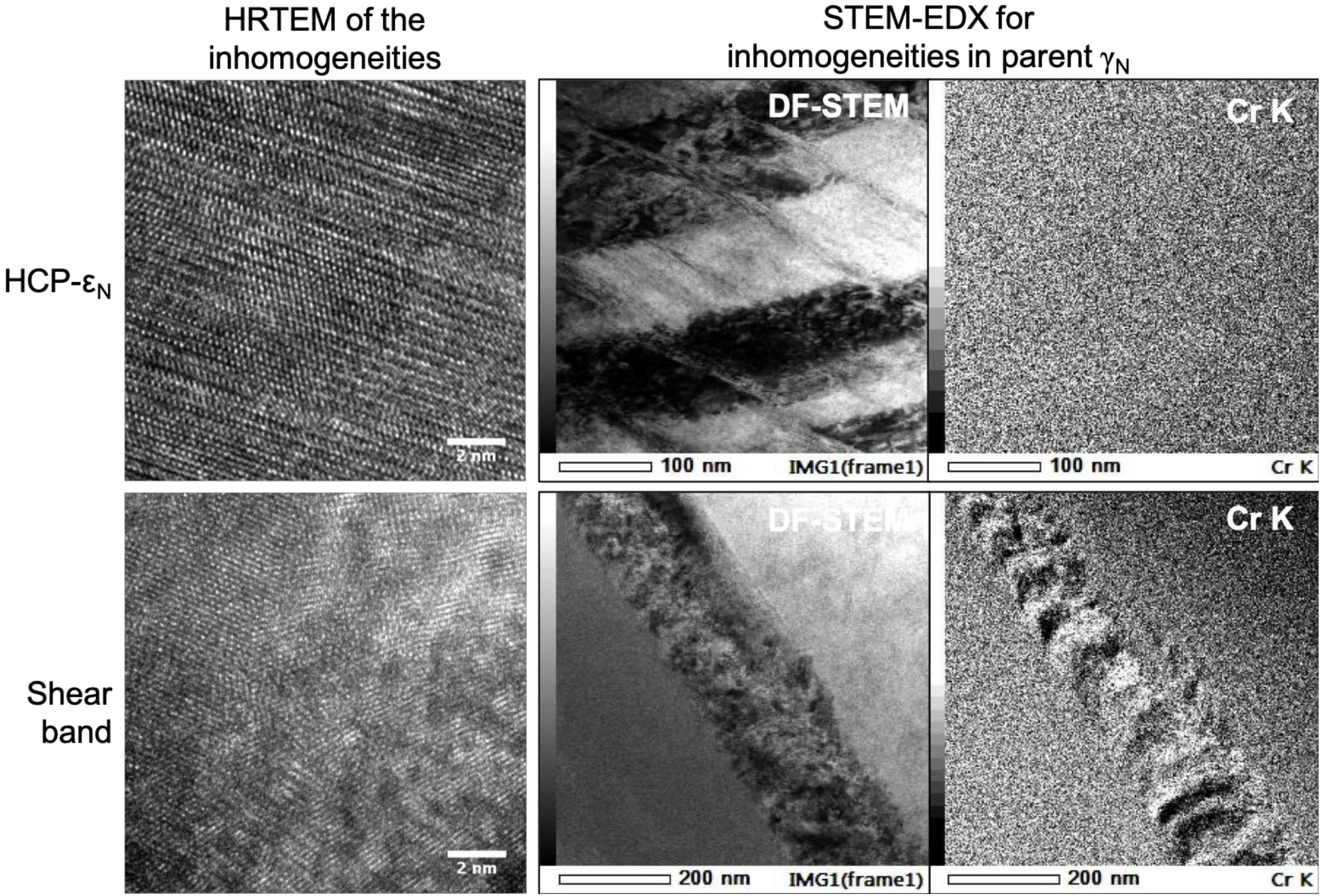

On the nitrogen interstitial induced lattice inhomogeneities in nitrogen-expanded austenite

Authors:

Xiao Tao[a, c], Jiahui Qi[a], Mark Rainforth[a], Allan Matthews[b], Adrian Leyland[a]

[a] Department of Materials Science and Engineering, The University of Sheffield, Sheffield, S1 3JD, UK

[b] School of Materials, The University of Manchester, Manchester, M13 9PL, UK

[c] School of Metallurgy and Materials, University of Birmingham, Birmingham B15 2TT, UK

Abstract

Lattice inhomogeneities, i.e. nitrogen interstitial-induced hexagonal-close-packed martensite (HCP-ε_N) and shear bands, can form in face-centred cubic nitrogen-expanded austenite (FCC-γ_N) synthesised on Fe-Cr-Mn and Fe-Cr-Ni austenitic stainless steel (ASS) using triode-plasma nitriding (TPN). Homogenous elemental distribution between HCP-ε_N and FCC-γ_N supports the displacive shear transformation mechanism proposed for a high-Mn, low stacking fault energy ASS under nitrogen interstitial-induced deformation. While being a product of transformation-induced plasticity effect, HCP-ε_N exhibits similar lattice expansion behaviour to the parent FCC-γ_N. However, inhomogeneous elemental distributions in the shear bands formed in γ_N layers on a 400°C TPN-treated high-Ni ASS indicate local migration of substitutional elements.

Keyword: nitriding; expanded austenite; shear banding; martensitic phase transformation; high-resolution electron microscopy (HREM)

Low temperature thermochemical diffusion treatments have been developed as an important and effective surface engineering method to improve the wear resistance of austenitic stainless steels (ASSs), generating hard, yet corrosion resistant surface layers supersaturated with interstitial nitrogen and/or carbon, named 'expanded austenite' or 'S-phase' [1-5]. A metastable, expanded face-centred cubic (FCC) phase appears to be the most plausible and widely applicable interpretation so far for this type of interstitially-supersaturated material formed on ASSs under low temperature diffusion treatment, with a widely used designation 'γ_N' and 'γ_C' (when supersaturated with nitrogen and carbon, respectively) [6-10]. After prolonged treatment at 'low' temperatures (these being typically below ~450°C for nitrogen and ~550°C for carbon), an excessive concentration of interstitial atoms is diffused into the substrate near-surface (e.g. up to ~38 at.% N in AISI 316 ASS [8]) which, although many times the expected equilibrium solubility limit in ASSs, does not lead to direct phase transformation of the original FCC structure.

Following the work of Ichii et al. in 1986 [11], the anomalous XRD peak shifting and anisotropic lattice expansion of γ_N has been known and investigated for many years. The lattice expansion anomalies observed have been attributed to stacking fault (SF) generation and to the hkl-dependent (anisotropic) 'deformation' behaviour of FCC material in elastic and/or plastic deformation regimes (i.e. accommodation of supersaturated concentrations of nitrogen and/or carbon elasto-plastically) [6, 7, 10]. A more recent study [12] reveals anisotropic lattice rotation for AISI 316 ASS after low temperature nitriding using electron backscatter diffraction (EBSD), where a reasonably good correlation was found between nitrogen composition-induced anisotropic lattice rotation and out-of-plane tensile deformations, that could be simulated using the Taylor-Bishop-Hill model [13].

Under transmission electron microscopy (TEM), γ_N has often been reported to contain a large number of lattice defects, e.g. dislocations, nanotwins and stacking faults (SFs) [14-19]. These crystallographic defects can interrupt the local crystallinity of γ_N, but do not necessarily alter the underlying crystal structure. Recently it was proposed that, similar to FCC materials under mechanical deformation, the observed interstitial supersaturation-induced deformation mechanisms (and their prevalence) could depend on the materials stacking fault energy (SFE) [20]. Hexagonal-close-packed (HCP) ε_N [19, 20] and shear bands [20] could form in γ_N layers when a large amount of such defects accumulate locally, causing the underlying

crystallographic structure to be severely interrupted (and/or altered) over comparatively large lengthscales. The "mono-phased" metastable nitrogen diffusion layer could contain inhomogeneous regions (formed predominately via chemical composition-mediated deformation phenomena, occurring during/after low temperature thermochemical diffusion treatments) in place of, or prior to, the known nitride phase precipitation, that occurs at more elevated treatment temperatures and/or prolonged treatment times. A good understanding of these 'deformation'-mediated inhomogeneities (although not likely to be found in 'Cr-free' γ_N [21] at comparatively low interstitial supersaturation levels) would provide valuable insights into the structure (and process-structure-property relationships) of metastable, interstitially highly-supersaturated, anisotropically-expanded austenite(s).

The nominal compositions of Staballoy AG17® and RA 330® are Fe-17Cr-20Mn-0.5N and Fe-19Cr-35Ni, respectively. In this work, both alloys were treated under triode-plasma nitriding (TPN) at 400°C for 20hrs (-200V substrate bias, 0.4 Pa chamber pressure and 7:3 N_2:Ar gas volumetric ratio); detailed property characterisation and nanostructural studies are reported elsewhere [20]. For the results presented here, thin foils were prepared (in cross-section) from the treated surfaces by focused ion beam (FIB) milling, using an FEI Quanta 200 3D instrument (with Gallium ion beam). In this investigation, high-resolution TEM (HRTEM) images were obtained from the prepared foils using a cold field emission gun (C-FEG) JEOL R005 double aberration corrected TEM operating at 300 kV. Scanning TEM (STEM) imaging and energy-dispersive X-ray (EDX) elemental mapping at high point-to-point resolution was carried out using a C-FEG JEOL F200 microscope at 200 kV (with twin, solid state, ultra-sensitive silicon drift X-ray detectors). EDX data was analysed using Analysis Station 4 software provided by JEOL. Glancing angle X-ray diffraction (GAXRD) was carried out at 2° incident angle using a PANalytical Xpert3 diffractometer (with monochromated Cu$K\alpha_1$ 0.15406 nm), at 45 kV and 40 mA.

In the γ_N-AG17 layer synthesised on alloy AG17 after TPN at 400°C and 20hrs, the stacking sequences change from ABCA… in FCC-γ_N (**Fig. 1b**) to ABAB… in HCP-ε_N (**Fig. 1c**). The FCC-γ_N and HCP-ε_N interfaces follow a Shoji-Nishiyama orientation relationship, i.e. $\gamma_N(111)//\varepsilon_N(0002)$. The inverse FFT images (**Fig. 1d, e**) signify that the close-packed planes of neither γ_N nor ε_N appear as continuous straight lines − that may be attributed to the defects generated during the insertion of interstitial nitrogen. The interplanar spacings of $\gamma_N(111)$ and

ε_N(002) are approximately the same under HRTEM (**Fig. 1b, c**) at ~0.219 nm. One could estimate that $a_{\gamma N} = d_{\gamma N\,(hkl)} \times \sqrt{h^2 + k^2 + l^2} = 0.379\,nm$, $a_{\varepsilon N} = \frac{\sqrt{2}}{2} a_{\gamma N} = 0.268\,nm$ and $c_{\varepsilon N} = 2 \times d_{\gamma N\,(111)} = 0.438\,nm$ ($a_{\gamma N}$ is the lattice parameter for γ_N; $a_{\varepsilon N}$ and $c_{\varepsilon N}$ are the lattice parameters for ε_N, where $c_{\varepsilon N}/a_{\varepsilon N} \sim 1.63$).

STEM-EDX analysis suggests a homogenous elemental distribution in the TPN 400°C/20hrs treated AG17 sample (**Fig. 2a-f**), that is self-consistent to the previously proposed displacive martensitic shear transformation mechanism for the formation of HCP-ε_N in expanded austenite [20]. Evidenced by the homogenous N distribution seen in **Fig. 2f**, ε_N regions have a nitrogen content equivalent to the γ_N matrix at the same depth in the diffusion layer, and may also possess a decreasing nitrogen concentration-depth profile in the treatment layer, similar to γ_N. The formation of HCP-ε_N would start from (and require a minimum composition-induced lattice deformation at) some nitrogen concentration threshold. Thus, ε_N should have a composition window that overlaps with that of γ_N at higher nitrogen concentration levels.

More importantly, both γ_N and ε_N peaks are evident under GAXRD (**Fig. 3**). Taking the γ_N(111) peaks at ~40.93° and ~39.52° in **Fig. 3**, one could calculate that $a_{\gamma N} = \sim 0.382\,nm$ and $a_{\gamma N} = \sim 0.395\,nm$ after 4hrs and 20hrs of TPN, respectively. Taking the S-N orientation relationship and $d_{\gamma N\,(111)} = d_{\varepsilon N\,(002)}$, the lattice parameters for ε_N can be estimated as $a_{\varepsilon N} = \sim 0.270\,nm$ and $c_{\varepsilon N} = \sim 0.441\,nm$ after 4hrs of TPN, and $a_{\varepsilon N} = \sim 0.279\,nm$ and $c_{\varepsilon N} = \sim 0.456\,nm$ after 20hrs of TPN. The estimated peak positions of ε_N, strikingly, match well with those observed (hence, indexed) in **Fig. 3**. Noticeably, the X-ray attenuation depth (estimated using AbsorbDX software) on untreated alloy AG17 is ~0.4 μm under GAXRD at 2° glancing angle and ~2-3 μm under θ-2θ geometry. The observation of ε_N peaks under GAXRD in this study (but not under θ-2θ XRD, as in Ref. [20]) is believed to be due to the large volume fraction of ε_N in the uppermost regions of the diffusion layer.

In good agreement with the increasing volume fraction of ε_N with treatment time at 400°C [20], the relative intensity of the ε_N(101) reflection increases from 4hrs to 20hrs (**Fig. 3**). Most importantly, comparing with γ_N, HCP-ε_N also shows increasing peak shifts to lower 2θ angles with treatment time, indicating that ε_N undergoes similar lattice expansion under interstitial nitrogen absorption. Based on this peak-shift behaviour – and the dilated crystal structure that causes it – HCP-ε_N phase may tentatively be named as "expanded martensite". However,

whereas γ_N forms from unexpanded γ via N absorption, ε_N likely forms directly from γ_N (and not from unexpanded ε) through a composition-induced martensitic shear transformation above some critical N-concentration. Based on its formation mechanism, ε_N could therefore be categorised as a special deformation-induced martensite (DIM) with expanded lattice parameters formed under composition-induced deformation, in contrast to 'conventional' DIMs formed under mechanical deformation. Since the expanded lattice of γ_N would "shrink" under low-temperature annealing, ε_N very likely exhibits similar reversibility in expansion/contraction. The nitrogen composition-induced martensitic transformation from γ_N to ε_N could also be reversible upon the loss of interstitial nitrogen. In either case, the level of compressive residual stress (established under supersaturation and loss of interstitial nitrogen) would play a determining role. These arguments imply the need for further studies on the reversibility of plasticity mechanisms in γ_N; e.g. via low-temperature annealing of TPN-treated layers (carried out in combination with residual stress and chemical composition analysis).

Noticeably, owing to stress relaxation during TEM sample thinning, the lattice parameters estimated based on HRTEM are systematically smaller than those estimated based on XRD measurement. The lattice parameters of ε_N, if estimated using the $\gamma_N(200)$ peak positions instead of $\gamma_N(111)$, give ε_N peak positions at 2θ angles slightly lower than those observed from GAXRD. Although the true lattice parameters of γ_N are difficult to determine with precision, a plausible HCP-ε_N structure is proposed based on the $\gamma_N(111)$ XRD peak position, that gives satisfactory explanation to GAXRD profiles. However, the true structure of ε_N may deviate from the estimated one, considering the defects in both ε_N and γ_N implied by **Fig. 1(d, e**), and the high residual stress developed in the diffusion layer.

Owing to twinning-induced plasticity (TWIP) and/or transformation-induced plasticity (TRIP) effects, low-SFE alloys are known for their good uniform plastic ductility with continuous working hardening and delayed necking upon deformation, while γ_N-316 layers synthesised at high nitriding potential have been seen to show a tendency to crack [22]. With the ability to undergo martensitic shear transformation and local strain hardening, the composition induced plastic deformation could be distributed more uniformly within the surface treatment layer on alloy AG17, i.e. that TPN-treated low-SFE substrates may accommodate a higher amount of (composition induced) strain than high-SFE ones, without "failure". Compared to the localised shear bands and micro-cracks seen in γ_N-330 [20], the large amount of ε_N phase in γ_N-AG17

158 appears to "share" the composition-induced deformation. Additionally, substantial HCP-ε_N is
159 found in γ_N-AG17 [20] (and most likely occurs also in γ_N synthesised on other low-SFE
160 substrates), with such treatment layers possessing a duplex γ_N/ε_N microstructure. The nitrogen
161 interstitial-induced TRIP effect (and the unique duplex microstructure formed) could have a
162 complex and profound influence on material mechanical properties.
163
164 Low-temperature thermochemical diffusion treatments (such as carburising and nitriding) have
165 long been studied (and used) as hard protective surface layers for metallic components from
166 the aspect of Surface Engineering. Nevertheless, Ren Zheng et al. [23, 24] recently
167 demonstrated the unique intrinsic properties of γ_C-316. As the size of the "substrate" reduces,
168 the diffusion-treated layers play an increasingly important role in the performance of the bulk
169 component. The insertion of interstitials (such as carbon and nitrogen) into the parent lattice
170 via low-temperature thermochemical diffusion treatments could be exploited to tailor material
171 strength-ductility and/or other properties for small or thin-section components (such as medical
172 stents). However, although contributing to improved bulk yield strengths, the γ_C-316 layers
173 synthesised on both sides on thin AISI 316 foils (of thicknesses ranging from ~27 μm to ~100
174 μm) after carburising exhibited reduced ductility, showing brittle cleavage fracturing under
175 tensile testing [23]. AISI 316 foil (~20 μm thick) was also reported as fracturing into powder
176 during low-temperature nitriding [7]. Brittle fracturing limits the use of these interstitial-
177 supersaturated materials (i.e. both γ_N-316 and γ_C-316), typically when the "substrates" are
178 small. In this regards, the crack-free γ_N-AG17 layer synthesised (as compared to the crack-
179 containing γ_N-330) [20] and the nitrogen composition-induced TRIP effect provide new
180 insights on potentially breaking the strength-ductility trade-off, towards exploiting these
181 interstitially-supersaturated materials in bulk.
182
183 In contrast to ε_N, shear bands in γ_N (with localised strain and high 'stored' strain energy under
184 the nitrogen composition introduced deformation) appear to be problematic in terms of the
185 micro-cracking observed along them (as in [20]). **Fig. 4** shows the distorted and discontinuous
186 lattice fringes inside this shear band. FFT image suggests a strained and somewhat
187 polycrystalline sub-structure. The elemental distribution, while appearing rather homogenous
188 for parent γ_N-330, is inhomogeneous within the shear band (**Fig. 2g-l**), indicating redistribution
189 of both substitutional and interstitial atoms. While the relatively low treatment temperature at
190 400°C for this sample limits diffusion of substitutional elements [5], the local migration of such

elements within shear bands might be facilitated by the high defect density and/or the intensive shear stress. Additionally, Cr and N atoms tend to agglomerate in accordance to their high chemical affinity, and an associated rejection of Ni and Fe atoms. In EDX line profile (**Fig. 2h**), Cr content tends to increase with N content, but decreases with increasing Ni and Fe content. The bright areas in **Fig. 2j** and **Fig. 2l** (i.e. of high Cr and N content) appear dark in **Fig. 2i** and **Fig. 2k** (i.e. low Fe and Ni content, respectively). This element segregation in shear bands in the γ_N-330 layer raises concerns about material corrosion performance, as the local low-Cr volumes could be more vulnerable to galvanic attack and may result in pitting or (when combined with the micro-crack network) crevice corrosion.

Nevertheless, there is currently no direct evidence of the formation of a stoichiometric CrN nitride phase within shear bands in γ_N-330 layers after 400°C nitriding (see [20] and GAXRD profiles in **Appendix**). The 3rd EDX spot (along the scan direction in **Fig. 2g**) shows the lowest (but still significant) Ni content (**Fig. 2h**). Given the high Fe and Ni content still in the high Cr regions (**Fig. 2h**) and considering the prohibited substitutional migration at 400°C, it is anticipated that the observed elemental re-distribution is moving towards thermodynamic equilibrium, but still in a paraequilibrium state [25], without stoichiometric CrN compound phase formation. The paraequilibrium phase(s) could have slightly different lattice parameter(s) to the parent γ_N-330. Additionally, the minor alloying elements in the substrate (i.e. 1.4 wt.% Mn, 1.2 wt.% Si, 0.16 wt.% Al, 0.14 wt.% Ti, 0.11 wt.% Cu and 0.05 wt.% C) could have migrated and played important roles in the formation of these intermediate phase(s). Rejection of Mn from high-Ni regions and Si redistribution was observed within a shear band after more extensive STEM-EDX analysis (see **Appendix**). Probably owing to their small amounts, the re-distribution of Al, Ti, Cu and C (although likely to have occurred) cannot clearly be seen.

In this paper, we investigated the structure and local chemical composition of the HCP-ε_N regions and shear bands in the metastable nitrogen diffusion layers on two special ASSs using advanced TEM analysis. The evident ε_N/γ_N duplex structure under HRTEM and the homogenous elemental distribution under STEM-EDX in the γ_N-AG17 TPN layer is consistent to the previously proposed nitrogen-composition induced displacive shear transformation mechanism. HCP-ε_N 'expands' in accompaniment with γ_N and might be named as 'nitrogen-expanded martensite'. On the other hand, the inhomogeneous elemental distribution in shear bands in the γ_N-330 TPN layer indicates segregation of substitutional elements – even at a low

nitriding temperature of 400°C. Although there is no direct evidence of stoichiometric CrN in γ_N-330, volumes of different chemical composition found along shear bands suggest the formation of intermediate metastable phase(s). It is evident that local volumes of lattice inhomogeneity may form via displacive plasticity mechanisms in γ_N. Both nitrogen composition-induced ε_N formation and shear banding could disrupt the expanded FCC structure and would play a significant role in resulting material properties and performance. Nitrogen-composition induced TRIP effects might be exploited to achieve improved strength-ductility combinations, and permit the use of interstitially-supersaturated ASS materials in bulk form.

Acknowledgements

This work was supported by EPSRC project "Friction: The Tribology Enigma" (Grant EP/001766/1) and Henry Royce Institute for Advanced Materials at the University of Sheffield (Grant EP/R00661X/1, EP/S019367/1, EP/P02470X/1 and EP/P025285/1).

References

[1] Z.L. Zhang and T. Bell, Surf. Eng. 1 (1985) 131-136.
[2] S.P. Hannula, O. Nenonen, and J.-P. Hirvonen, Thin Solid Films. 181 (1989) 343-350.
[3] A. Leyland, D.B. Lewis, P.R. Stevenson, and A. Matthews, Surf. Coat. Technol. 62 (1993) 608-617.
[4] M.A.J. Somers and T. Christiansen, Low temperature surface hardening of stainless steel in: E.J. Mittemeijer and M.A.J. Somers (Eds.), Thermochemical Surface Engineering of Steels, Woodhead Publishing: Cambridge. 2015, pp. 557-579.
[5] D.L. Williamson and O. Ozturk, Surf. Coat. Technol. 65 (1994) 15-23.
[6] Y. Sun, X.Y. Li, and T. Bell, J. Mater. Sci. 34 (1999) 4793-4802.
[7] T. Christiansen and M.A.J. Somers, Scripta Mater. 50 (2004) 35-37.
[8] T. Christiansen and M.A.J. Somers, Metall. Mater. Trans. A. 37A (2006) 675-682.
[9] T.S. Hummelshoj, T.L. Christiansen, and M.A.J. Somers, Scripta Mater. 63 (2010) 761-763.
[10] B.K. Brink, K. Stahl, T.L. Christiansen, J. Oddershede, G. Winthiner, and M.A.J. Somers, Scripta Mater. 131 (2017) 59-62.
[11] K. Ichii, K. Fujimura, and T. Takase, Technol. Rep. Kansai Univ. 27 (1986) 135-144.
[12] J.C. Stinville, P. Villechaise, C. Templier, J.P. Riviere, and M. Drouet, Acta Mater. 58 (2010) 2814-2821.
[13] J.C. Stinville, J. Cormier, C. Templier, and P. Villechaise, Acta Mater. 83 (2015) 10-16.
[14] J.C. Jiang and E.I. Meletis, J. Appl. Phys. 88 (2000) 4026-4031.
[15] X.L. Xu, L. Wang, Z.W. Yu, and Z.K. Hei, Surface & Coatings Technology. 132 (2000) 270-274.
[16] X.Y. Li and Y. Sun, Transmission electron microscopy study of S phase in low temperature plasma nitrided 316 stainless steel, in: T. Bell and K. Akamatsu (Eds.),

Stainless Steel 2000: Thermochemical Surface Engineering of Stainless Steel, Maney Publishing: London. 2001, pp. 215-228.
[17] E.I. Meletis, V. Singh, and J.C. Jiang, J. Mater. Sci. Lett. 21 (2002) 1171-1174.
[18] D. Stroz and M. Psoda, J. Microsc. (Oxford, U. K.). 237 (2010) 227-231.
[19] K. Tong, F. Ye, H. Che, M.K. Lei, S. Miao, and C. Zhang, J. Appl. Crystallogr. 49 (2016) 1967-1971.
[20] X. Tao, X. Liu, A. Matthews, and A. Leyland, Acta Mater. 164 (2019) 60-75.
[21] X. Tao, A. Matthews, and A. Leyland, Metall. Mater. Trans. A. 51 (2020) 436-447.
[22] T. Christiansen and M.A.J. Somers, Surf. Eng. 21 (2005) 445-455.
[23] Z. Ren, A.H. Heuer, and F. Ernst, Acta Mater. 167 (2019) 231-240.
[24] Z. Ren and F. Ernst, Acta Mater. 173 (2019) 96-105.
[25] G.M. Michal, X. Gu, W.D. Jennings, H. Kahn, F. Ernst, and A.H. Heuer, Metall. Mater. Trans. A. 40 (2009) 1781-1790.

Figure 1

Fig. 1 a) HRTEM image at the surface of γ_N-AG17 layer; HRTEM images and respective fast Fourier transform (FFT) for b) FCC-γ_N and c) HCP-ε_N as indicated in dashed lines in **Fig. 1a**; d) Inverse FFT image for **Fig. 1b**, signifying the 111 and $\bar{1}11$ planes; e) Inverse FFT image for **Fig. 1c**, signifying the 0002 planes. The amorphous carbon layer (at top left corner in **Fig. 1a**) was deposited on the sample surface during the FIB preparation process to protect the underlying material surface from ion beam damage.

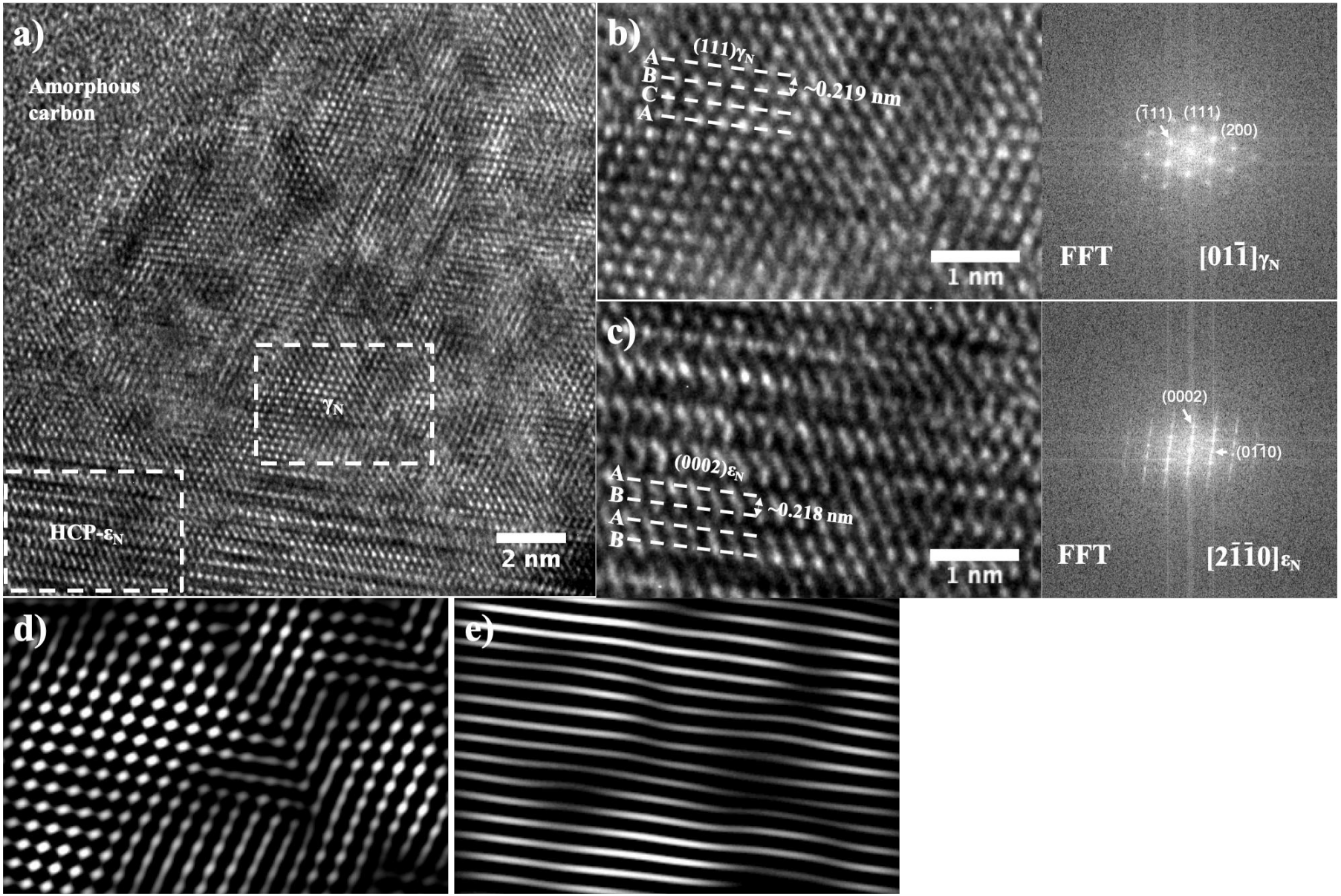

Figure 2

Fig. 2 DF-STEM images for HCP-ε_N regions in γ_N-AG17 (**Fig. 2a**) and a typical ~200 nm wide shear band in γ_N-330 (**Fig. 2b**); corresponding STEM-EDX maps for ε_N in γ_N-AG17 (**Fig. 2c-f**) and shear band in γ_N-330 (**Fig. 2i-l**); EDX line scans across ε_N (**Fig. 2b**) and shear band (**Fig. 2h**). EDX analysis was performed with respect to the main alloy elements (i.e. Fe, Cr, Mn, N for nitrided AG17 and Fe, Cr, Ni, N for nitrided 330). The EDX spots on the line scan are also presented in elemental maps in **Fig. 2i-l**.

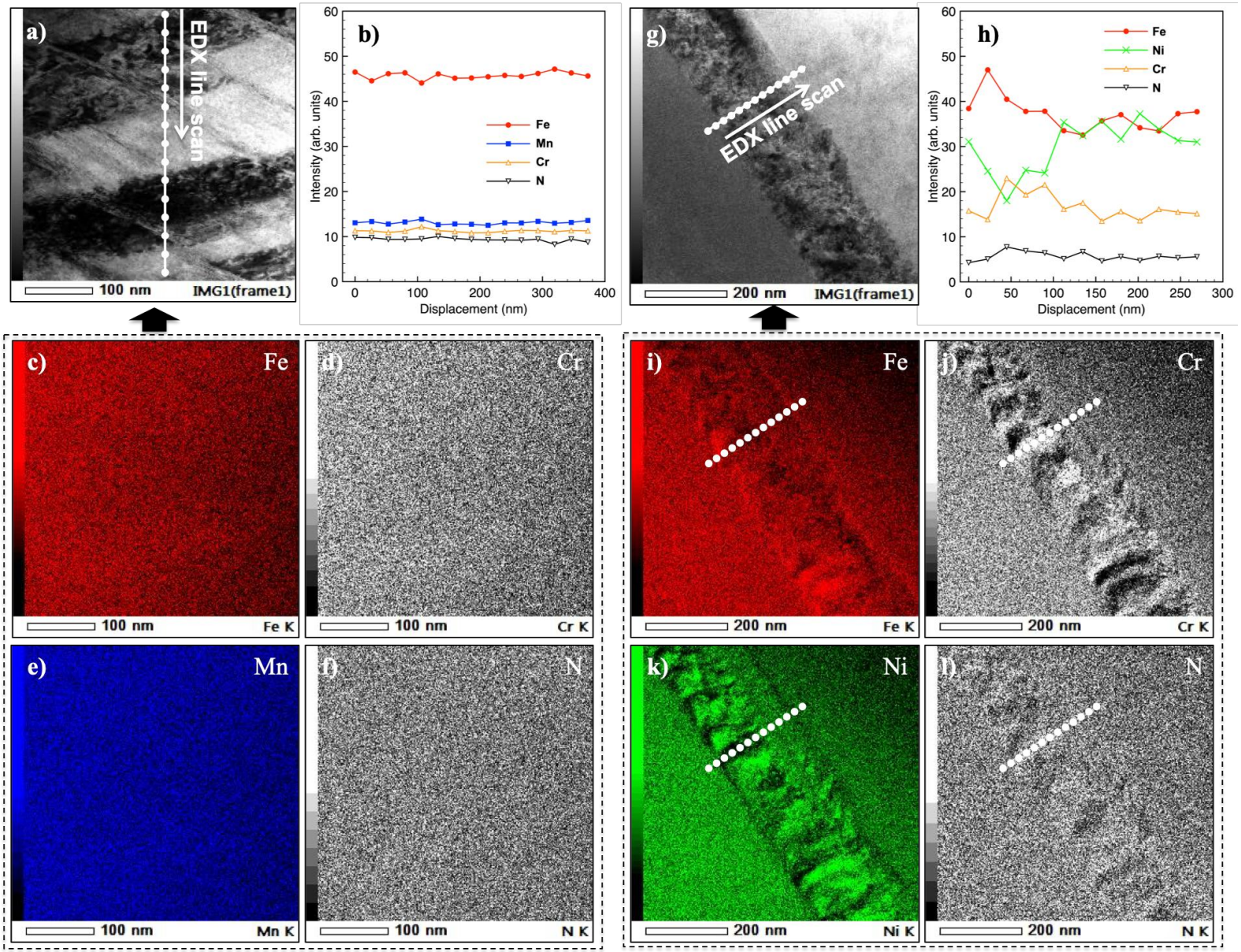

Figure 3
Fig. 3 GAXRD profiles of alloy AG17 before and after nitriding treatment at 400° C for 4hrs and 20hrs

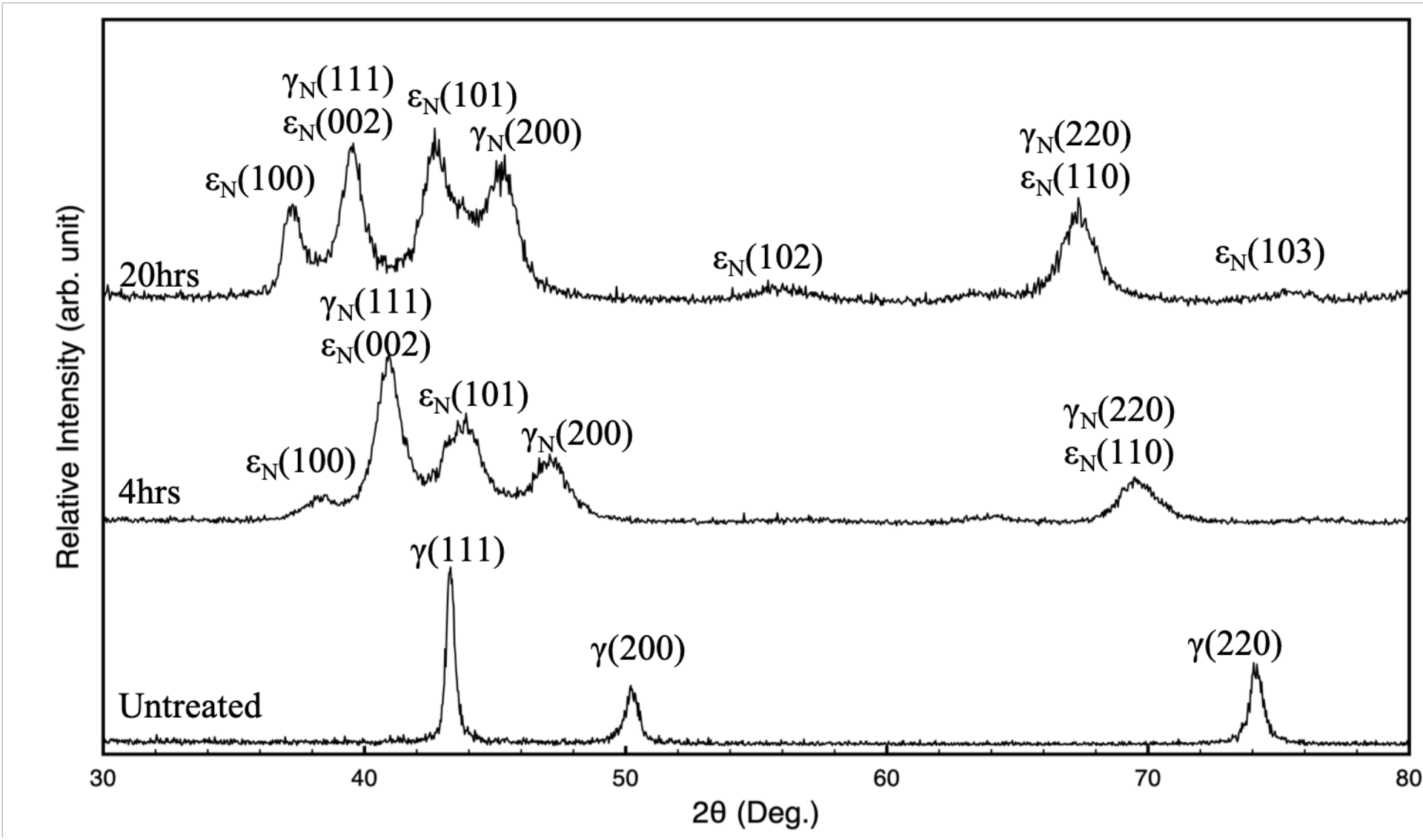

Figure 4

Fig. 4 HRTEM images inside a shear band in γ_N-330 layer and corresponding FFT

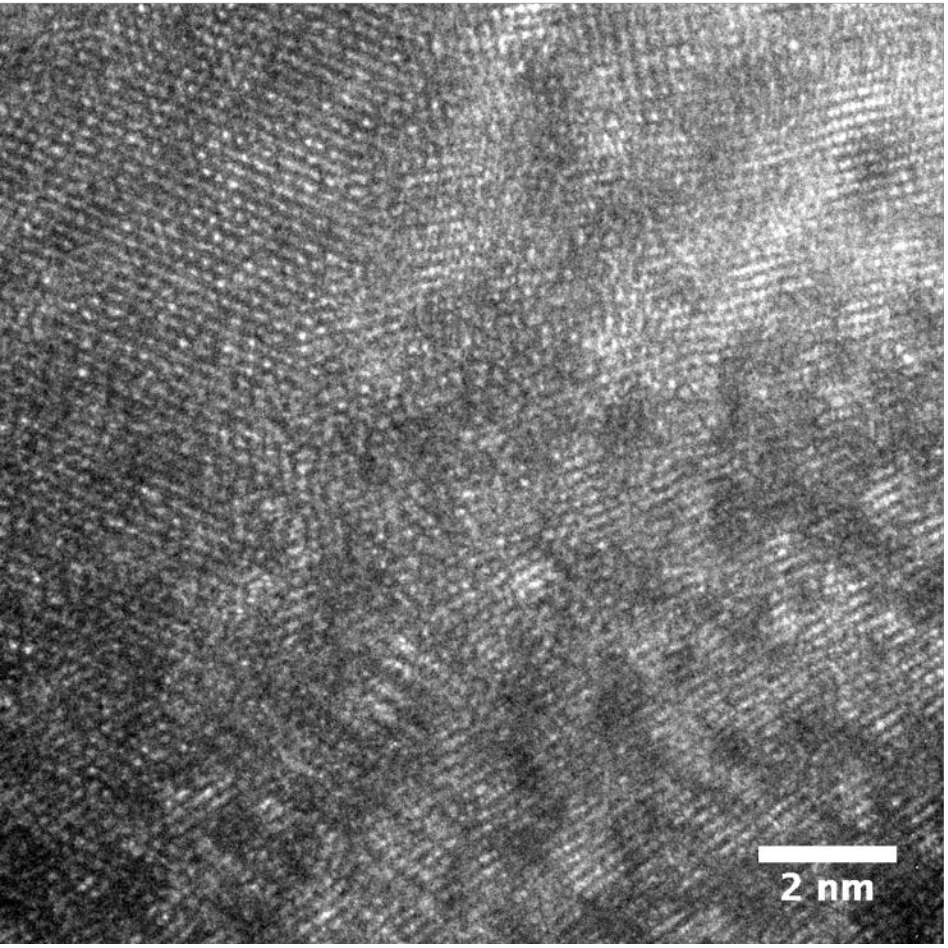

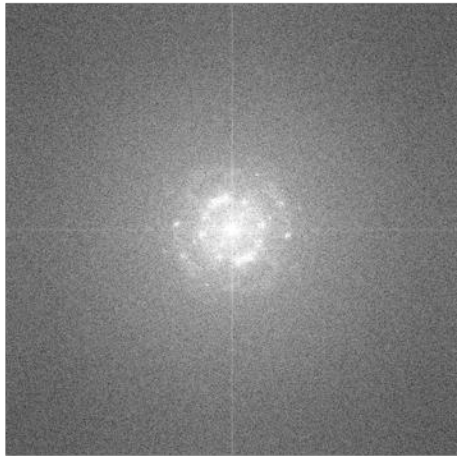

Appendix

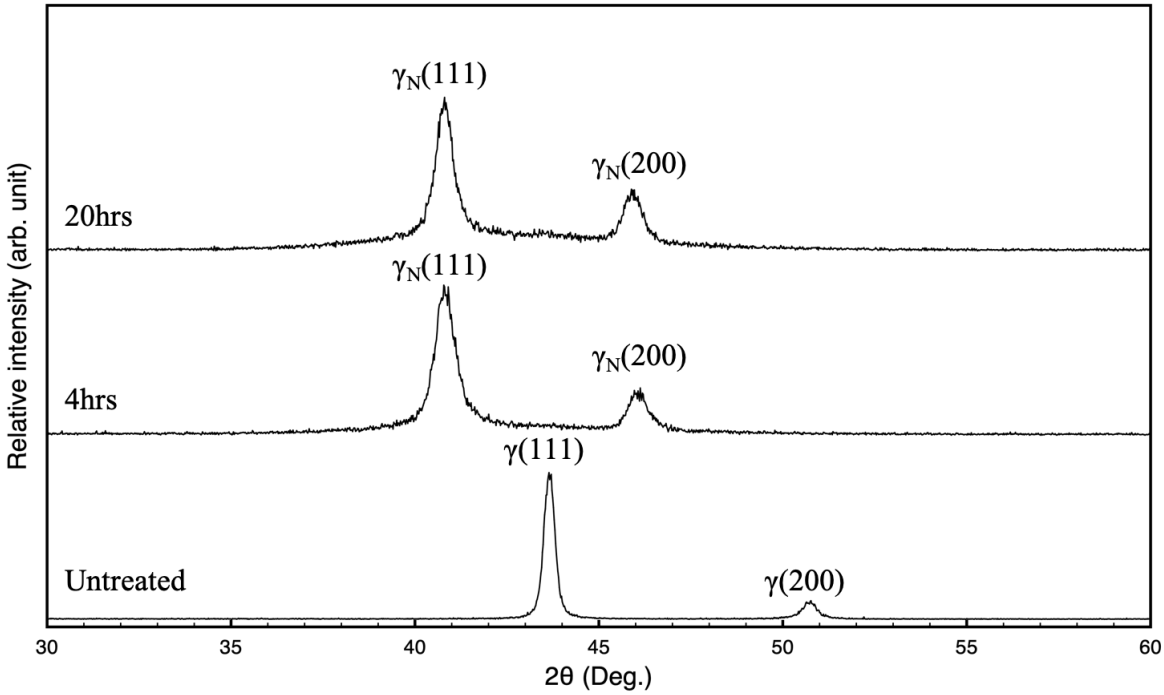

Fig. 1 GAXRD profiles of alloy 330 before and after nitriding treatment at 400°C for 4hrs and 20hrs. Only γ_N peaks were observed after TPN treatments. A saturated expansion was reached after 4hrs of TPN at 400°C.

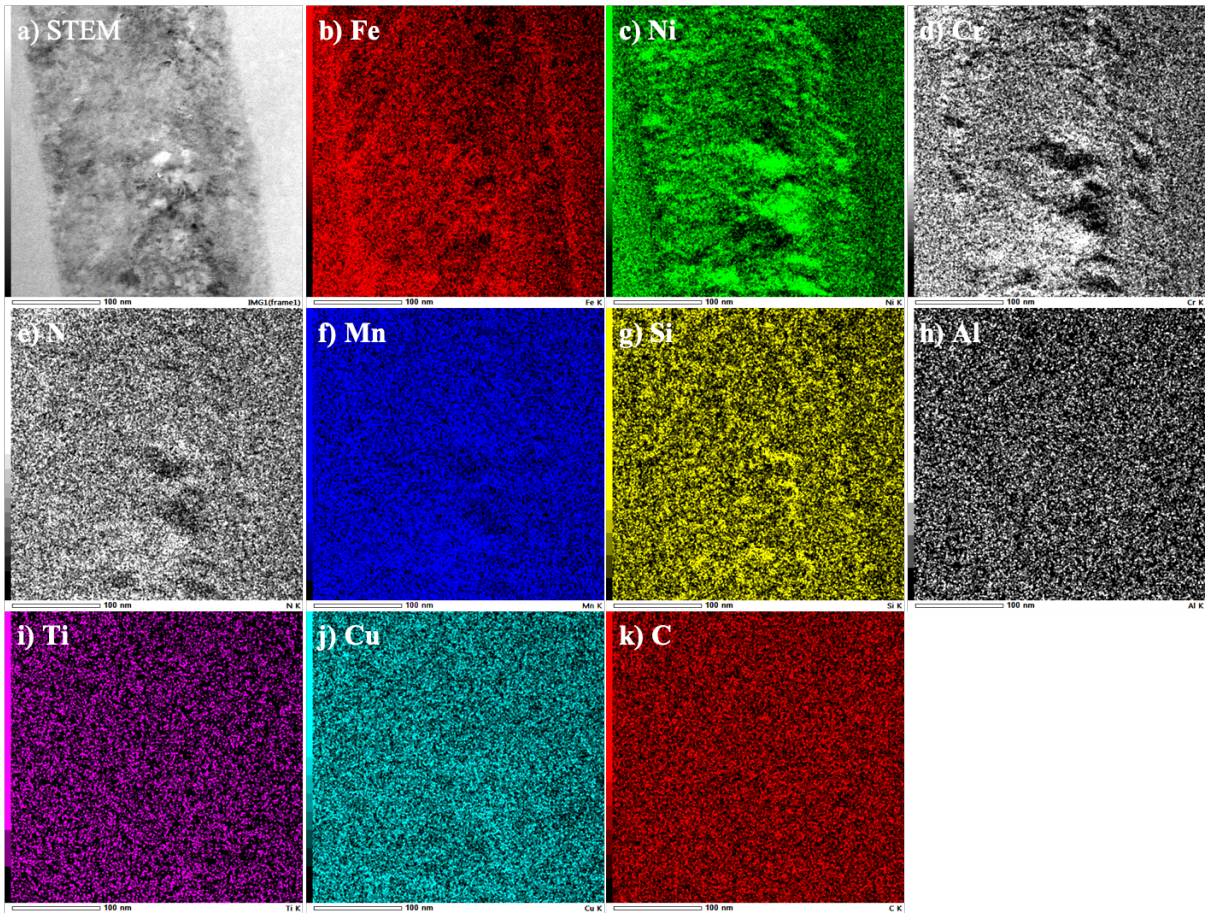

Fig. 2 STEM-EDX mapping for all elements in γ_N-330. a) BF-STEM image for the field of interest; STEM-EDX mapping for elements: b) Fe, c) Ni, d) Cr, e) N, f) Mn, g) Si, h) Al, i) Ti, j) Cu, and k) C. STEM-EDX conditions: C-FEG 200 kV, 10 µm C2 aperture, and Spot size 6.